RSC Chemical Biology

ROYAL SOCIETY OF CHEMISTRY

PAPER

View Article Online
View Journal | View Issue

Cite this: *RSC Chem. Biol.*, 2020, **1**, 421

Met80 and Tyr67 affect the chemical unfolding of yeast cytochrome *c*: comparing the solution *vs.* immobilized state

Alessandro Paradisi,[a] Lidia Lancellotti,[b] Marco Borsari,[b] Marzia Bellei,[c] Carlo Augusto Bortolotti,[c] Giulia Di Rocco,[c] Antonio Ranieri,[c] Marco Sola[c] and Gianantonio Battistuzzi*[b]

Urea-induced denaturation of the Met80Ala and Met80Ala/Tyr67Ala variants of *S. cerevisiae* iso-1 cytochrome *c* (ycc) was studied through variable temperature diffusive cyclic voltammetry and electronic absorption, CD and MCD spectroscopies. The susceptibility to unfolding of both variants – represented by the free energy of unfolding at denaturant infinite dilution, $\Delta G_u^{\circ H_2O}$ – is greater compared to the species showing an intact Met/His coordination, as observed previously for the same species immobilized onto a functionalized electrode. This is consistent with the role of the axial Fe–(S)Met bond and the H-bond network involving Tyr67 in stabilizing the polypeptide matrix in the heme crevice. Notably, we find that the unfolding propensity and axial heme iron coordination of the present Fe–(S)Met bond-deprived variants are affected by the motional regime of the protein. In particular, electrostatic adsorption onto a negatively charged SAM surface – which would mimic the phospholipidic inner mitochondrial membrane – facilitates unfolding compared to the solution state, especially at room temperature. This finding has physiological relevance related to the cytochrome *c* interaction with cardiolipin at the IMM in the early stages of apoptosis. Moreover, while both immobilized variants maintain the His/OH^- axial heme iron coordination up to 7 M urea, the same species in solution are subjected to urea-induced replacement of the axial hydroxide ligand by a His ligand. The contributions of the enthalpic and entropic terms to $\Delta G_u^{\circ H_2O}$ were found to be opposite (H–S compensation), indicating that the unfolding thermodynamics are strongly affected by changes in the hydrogen bonding network in the hydration sphere of the protein.

Received 3rd July 2020,
Accepted 17th August 2020

DOI: 10.1039/d0cb00115e

rsc.li/rsc-chembio

Introduction

Mitochondrial cytochrome *c* (cytc) is a small globular protein which shuttles electrons between cytochrome *c* reductase and cytochrome *c* oxidase in the mitochondrial intermembrane space.[1–7] It contains a single six-coordinate heme *c* wedged into a hydrophobic environment, which is axially coordinated by His18 and Met80.[1–7] The solution properties and binding events affect the heme environment and axial ligation,[1,3–5,8–27] modifying the physiological role *in vivo* and the reactivity *in vitro*.[1,5,9,13–16,18,19,28–40] Indeed, cytochrome *c* has proven to be a multi-tasking protein whose biological role is modulated by external stimuli and cell conditions.[1,4,28,30,41] The paradigm of this tunable functionality *in vivo* is the interaction with cardiolipin (CL), a negatively charged glycerophospholipid found in the inner mitochondrial membrane (IMM),[30,40,42] which induces the cleavage of the Fe–S(Met80) bond,[1,5,9,19,21,28,30,32,39,42–72] imparting to cytc significant (lipo)peroxidase activity, which is crucial in triggering the apoptosis cascade.[1,5,28,30,40,47,73] *In vitro*, analogous heme axial ligand swapping from His/Met to His/His occurs upon chemical denaturation of both solution[14] and surface-immobilized yeast cytochrome *c* (ycc).[14,33,34,74–77] Under the latter conditions, ycc gains remarkable pseudo-peroxidase activity.[32,34,75–77]

Because of their physiological relevance, the conformational equilibria leading to non-native states of cytochrome *c* have been studied in depth,[1,6,7,14,18,22,24–27,41,43,78–80] making it a model system widely used to unravel the mechanistic details of protein folding and unfolding.[5,8,9,22,23,25,38,41,78,81–84] In this work, we used a combination of spectroscopic and electrochemical techniques to analyze the urea-induced unfolding of the M80A and M80A/Y67A variants of ycc under freely diffusing

[a] *Department of Chemistry, University of York, Heslington, YO10 5DD, York, UK*
[b] *Department of Chemistry and Geology, University of Modena and Reggio Emilia, via Campi 103, 41126 Modena, Italy. E-mail: gianantonio.battistuzzi@unimore.it; Tel: +39-0592058639*
[c] *Department of Life Sciences, University of Modena and Reggio Emilia, via Campi 103, 41126 Modena, Italy*

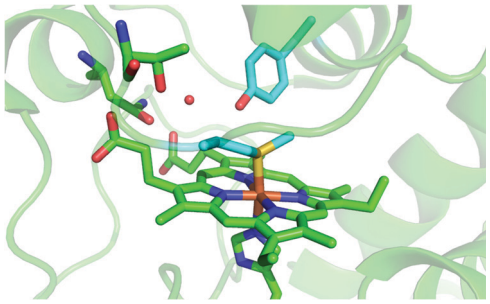

Fig. 1 Cartoon representing the heme environment in wild type yeast cytochrome *c* (PDB 3CYT) and highlighting the Met80 and Tyr67 residues in light blue.

conditions. The former mutation was selected to quantitatively assess the contribution of the distal axial heme ligation to the overall conformational stability of cytochrome *c*, whereas the evolutionary conserved Tyr67 was chosen because its OH group participates in the hydrogen bond (H-bond) network in the distal side of the heme connecting the Ω loops formed by residues 40–57 and 71–85 (Fig. 1),[85–96] which are the least stable foldons.[78,79] Therefore, Tyr67 plays a key role in stabilizing the three-dimensional structure of folded ycc and controlling the solvent accessibility to the heme crevice.[85–96] Moreover, Tyr67 was indicated as a possible apoptotic trigger.[85]

Previous studies showed that removal of the axial Met ligand enhances the pseudoperoxidase and nitrite reductase activity[97–99] and facilitates urea-induced unfolding of the SAM-immobilized proteins, preventing coordination of a second axial His ligand at high urea concentrations,[77] whereas suppression of Tyr67 induced significant urea-induced changes in protein solvation.[77] Moreover, axial heme iron ligation, the protein conformation, the solvation properties, the heme reduction potential and the pseudoperoxidase and nitrite reductase activity of immobilized ycc were found to be affected by the nature of the noncovalent protein–SAM interaction (either electrostatic or hydrophobic).[76,77] In this work, we compare the thermodynamics of urea-induced denaturation of ycc in solution *versus* the immobilized state to test the effect of constrained protein mobility on the susceptibility of ycc to chemical unfolding. We find that such a constraint favors unfolding. This finding recognizes an additional factor that contributes to the functional versatility and tunability of cytochrome *c* under physiological conditions.

Experimental

Materials

All chemicals were reagent grade. Doubly distilled water was used throughout. 4-Mercapto-pyridine was purchased from Sigma-Aldrich and used without further purification.

Protein production and isolation

The M80A and M80A/Y67A mutants of recombinant *S. cerevisiae* iso-1 cytochrome *c* were expressed and isolated as described previously.[95,97–100] All protein variants are nontrimethylated and carry the C102T mutation to prevent protein dimerization.[95,97–100]

Spectroscopic measurements

Electronic absorption, CD and MCD spectra were recorded with a Jasco J-810 spectropolarimeter. The magnetic field was provided by a GMW magnet system Model 3470 split coil superconductivity magnet with a maximum field of 1 Tesla (T). Both CD and MCD spectra were measured in θ = mdeg. The former were converted to molar ellipticity $[\theta]$ using the conversion factor $[\theta] = \theta(\mathrm{deg})\cdot 100/(d\cdot c)$, where c is the protein concentration (mol dm^{-3}) and d is the thickness of the sample (path length, 0.5 cm),[21,84,90] while the latter were converted to $\Delta\varepsilon$ $[M^{-1}\ cm^{-1}\ T^{-1}]$ using the conversion factor $\Delta\varepsilon = \theta/(32\,980\cdot c\cdot d\cdot B)$, where c is the protein concentration, B is the magnetic field (1 T), and d is the thickness of the sample (path length, 0.5 cm).[13,101–104] All experiments were carried out at 25 °C with protein solutions freshly prepared before use in 5 mM phosphate buffer pH 7 and the protein concentration was checked spectrophotometrically, using ε_{405} = 121 700 $M^{-1}\ cm^{-1}$ for both the M80A and M80A/Y67A mutants.[105,106]

Electrochemical measurements

Cyclic voltammetry (CV) measurements were carried out with a potentiostat/galvanostat mod. 273A (EG&G PAR, Oak Ridge, USA). Experiments were carried out at different scan rates (0.02–5 V s^{-1}) using a cell for small volume samples (0.5 mL) under argon. A polycrystalline gold wire functionalized with 4-mercapto-pyridine,[12,107] a platinum sheet, and a saturated calomel electrode (SCE) were used as the working, counter, and reference electrodes, respectively. The electric contact between the SCE and the working solution was achieved with a Vycor® (from PAR) set. Reduction potentials were calibrated against the ferrocene/ferrocenium couple under all experimental conditions employed in this work to make sure that the effects of liquid junction potentials were negligible. All reduction potentials reported here are given with reference to the standard hydrogen electrode (SHE). Protein solutions were freshly prepared before use in 10 mM phosphate buffer plus 100 mM sodium perchlorate at pH 7.2 and their concentration was carefully checked spectrophotometrically (with a Jasco mod. V-570 spectrophotometer). The urea concentration was varied between 0 and 6 M. The formal potentials $E^{\circ\prime}$ were calculated as the semisum of the anodic and cathodic peak potentials and were found to be almost independent of the scan rate in the range 0.02–2 V s^{-1}. The signals persist for several voltammetric cycles throughout the temperature range investigated. The experiments were performed at least two times and the $E^{\circ\prime}$ values were found to be reproducible within ±0.002 V. The current intensities are proportional to the square root of the scan rate, as expected for a diffusive electrochemical process (not shown).

Variable-temperature CV experiments were carried out using a "non-isothermal" cell, in which the reference electrode was kept at a constant temperature (21 ± 0.1 °C), whereas the half-cell containing the working electrode and the Vycor® junction

to the reference electrode was under thermostatic control with a water bath.[108–113] The temperature was varied from 5 to 35 °C. With this experimental configuration, the standard entropy change for heme Fe(III) to Fe(II) reduction in ycc ($\Delta S^{\circ\prime}_{rc}$) is given by:[108–110]

$$\Delta S^{\circ\prime}_{rc} = S^{\circ\prime}_{red} - S^{\circ\prime}_{ox} = nF\left(\frac{dE^{\circ\prime}}{dT}\right) \quad (1)$$

Thus, $\Delta S^{\circ\prime}_{rc}$ was determined from the slope of the plot of $E^{\circ\prime}$ *versus* temperature, which turns out to be linear under the assumption that $\Delta S^{\circ\prime}_{rc}$ is constant over the limited temperature range investigated. With the same assumption, the enthalpy change ($\Delta H^{\circ\prime}_{rc}$) was obtained from the Gibbs–Helmholtz equation, namely as the negative slope of the $E^{\circ\prime}/T$ *versus* $1/T$ plot.[11,111–113] The nonisothermal behavior of the cell was carefully checked by determining the $\Delta H^{\circ\prime}_{rc}$ and $\Delta S^{\circ\prime}_{rc}$ values of the ferricyanide/ferrocyanide couple.[110–113]

Results and discussion

Absorption and MCD spectra

The electronic absorption and MCD spectra of ferric M80A and M80A/Y67A in the Soret (360–450 nm) and in the visible (450–710 nm) regions at pH 7 in the absence of urea (Fig. 2 and 3 and Table 1) match those reported previously.[102] The spectra point to a 6-coordinate His/OH^- low spin (**LS1**) form as the major species.[76,77,98,99,102,105,106,114] However, the shoulder at 398 nm observed in the 2nd derivative absorption spectra of both proteins (Fig. 2c and d) indicates that a minor high-spin (**HS1**) form is also present.[13]

For both variants, the Soret band in the absorption spectra and the single trough in the corresponding 2nd derivative spectra slightly redshift upon urea addition (Fig. 2a–d and Table 1), whereas the shoulder in the 2nd derivative spectra at 398 nm disappears above 4 M urea (Fig. 2c and d and Table 1).

The symmetrical S-shaped MCD signal is associated with the Soret band. The Soret band corresponds to a $\pi \rightarrow \pi^*$ electronic transition of the porphyrin ring, which would be doubly degenarate under the ideal D_{4h} symmetry of the porphyrin system (acceptor π^* orbitals of e_g symmetry).[115] However, the asymmetry of the protein environment around the heme lifts this degeneracy, producing two different electronic transitions close in energy.[116] In the MCD spectra of low spin ferric hemes these two transions gain intensity through the C-term mechanism but have opposite signs and hence generate the characteristic S-shaped MCD signal of the Soret band.[117,118] The position and the overall shape of this MCD feature are not influenced by urea addition (Fig. 2e and f and Table 1), yet the peak-to-trough distance increases up to 4 M and 5 M urea for M80A and M80A/Y67A, respectively (Fig. 2e and f).

Furthermore, the α and β bands of both variants shift to shorter wavelengths (Fig. 3a and c and Table 1) and their intensity increases up to 5 M urea (Fig. 3a and c); the trough in the MCD spectra at 575 (M80A) and 573 (M80A/Y67A) nm is progressively replaced by a new trough at 568 and 565 nm, respectively, whereas the peak at 553 nm is replaced by a new peak at 547 nm (Fig. 3b and d and Table 1). No further spectral changes are observed above 4 M urea for M80A, while M80A/Y67A displays an intensity decrease above 7 M urea (Fig. 3). These spectral changes show that the major low-spin His/OH^--ligated form (**LS1**) and the minor high-spin form (HS1) observed in the absence of urea both transform into a second LS conformer (**LS2**) above 4 M urea (M80A) and 5 M urea (M80A/Y67A), whose spectroscopic features are consistent with the replacement of the axial hydroxide ligand by a His ligand (either His26 or His33),[1,19,27,33,34,39,43,44,62,66,119] as previously observed for wt ycc and its K72A/K73A/K79A mutant.[14,21] Hence, the behavior of freely diffusing M80A and M80A/Y67A markedly differs from that of the same species electrostatically immobilized on a MUA/MU SAM, which showed no change in the His/OH^- axial heme iron coordination up to 7 M urea.[77] The absence of further spectral changes at higher urea concentrations indicates that the His/His axial coordination of the **LS2** conformer of both mutants is remarkably stable.

The urea concentration that realizes half of the total absorbance changes at 570 and 520 nm in Fig. 4 (which would correspond to a 50% population of **LS1** and **LS2**) is about 2.2–2.3 M for both variants. These values are significantly lower than those reported for wt ycc (3.2 M and 3.5 M, at 25 °C and 5 °C, respectively[14,35]) and its K72A/K73A/K79A and K72A/K73H/K79A mutants (3.2 M and 3.1 M) at 5 °C,[14,75] indicating that removal of the Fe—Met80 bond favors the unfolding effect of urea. Hence, reduction of the structural constraints that connect the heme center to the polypeptide matrix due to removal of the Fe–Met80 bond lowers the protein resistance to chemical unfolding as found previously for the same immobilized on a MUA–MU SAM. This view is supported by the thermodynamics of unfolding (*vide infra*). The additional alteration of the network of H-bonding in the heme crevice due to the suppression of Tyr67 apparently exerts a negligible effect on the resistance of the freely diffusing protein to chemical unfolding.

Near-UV CD spectra

The near-UV (250–330 nm) CD spectrum of proteins consists of optically active heme transitions[120] and vibronic transition bands of the aromatic side chains.[121] This technique is particularly sensitive to structural changes in the environment of aromatic side chains in cytochromes *c*.[21,84,90,122–124] The CD spectrum of wt ferric ycc contains a number of small positive bands around 256 nm, arising from tyrosine side chains,[21] a broad positive band around 264 nm, attributed to porphyrin transitions,[122] and two sharp negative bands at 282 and 289 nm, assigned to transitions involving the Trp-59 side chain.[21,84,122] The near-UV CD spectra of M80A and M80A/Y67A (Fig. 5) are almost superimposable on that of wt ycc, indicating that neither deletion of the axial Met80 ligand nor changes in the H-bond network surrounding the heme induced by Tyr67 replacement significantly modify the protein folding.[21,84,90] Urea addition simplifies the CD spectrum of both mutants (Fig. 5), as the two sharp negative bands at 282

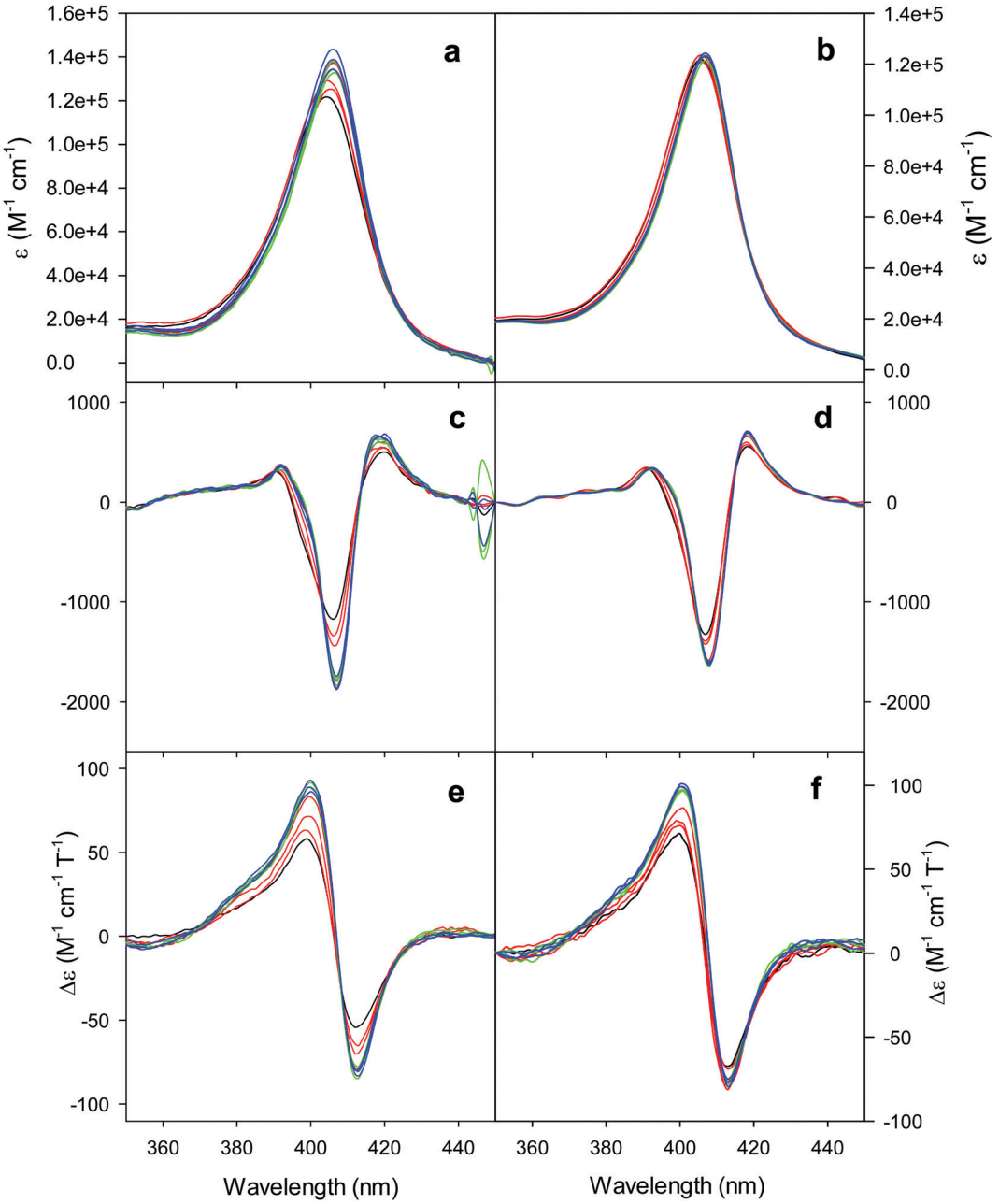

Fig. 2 Electronic absorption, 2nd derivative electronic absorption and MCD spectra in the Soret region for the oxidized M80A (a, c and e) and M80AY67A (b, d and f) variants of *S. cerevisiae* iso-1 cytochrome *c* in 5 mM phosphate buffer at pH 7 in the presence of increasing urea concentration: 0 M (black); 1, 2, and 3 M (red); 4, 5, and 6 M (green); and 7, 8, and 9 M (blue).

and 289 nm progressively decrease in intensity and disappear above 4 M urea, while the two maxima at 255 and 259 nm are replaced by a more intense maximum around 258 nm. These changes suggest that disruption of the tight packing of core residues occurs in both mutants upon increasing the urea concentration up to 5 M. No significant changes are observed at higher urea concentrations.

Voltammetric response

The cyclic voltammograms for freely diffusing M80A and M80A/Y67A at pH 7.2 show quasi-reversible signals arising from the one-electron reduction/oxidation of the heme iron (Fig. 6). The $E^{\circ\prime}$ values of −0.170 and −0.196 V obtained at pH 7.2 and 293 K for M80A and M80A/Y67A, respectively (Table 2), compare well with previous data for the same species immobilized on a polycrystalline gold electrode coated with a 1 : 1 mixed SAM of MUA and MU,[77,98,99] if we take into account the electrostatic stabilization of the ferric form by the negatively charged SAM.[98,99,125] Both the freely diffusing and immobilized variants feature a His/OH^- axial heme iron coordination set.[76,77,97–99] The voltammetric response and the temperature dependence of $E^{\circ\prime}$ were studied at varying urea concentration

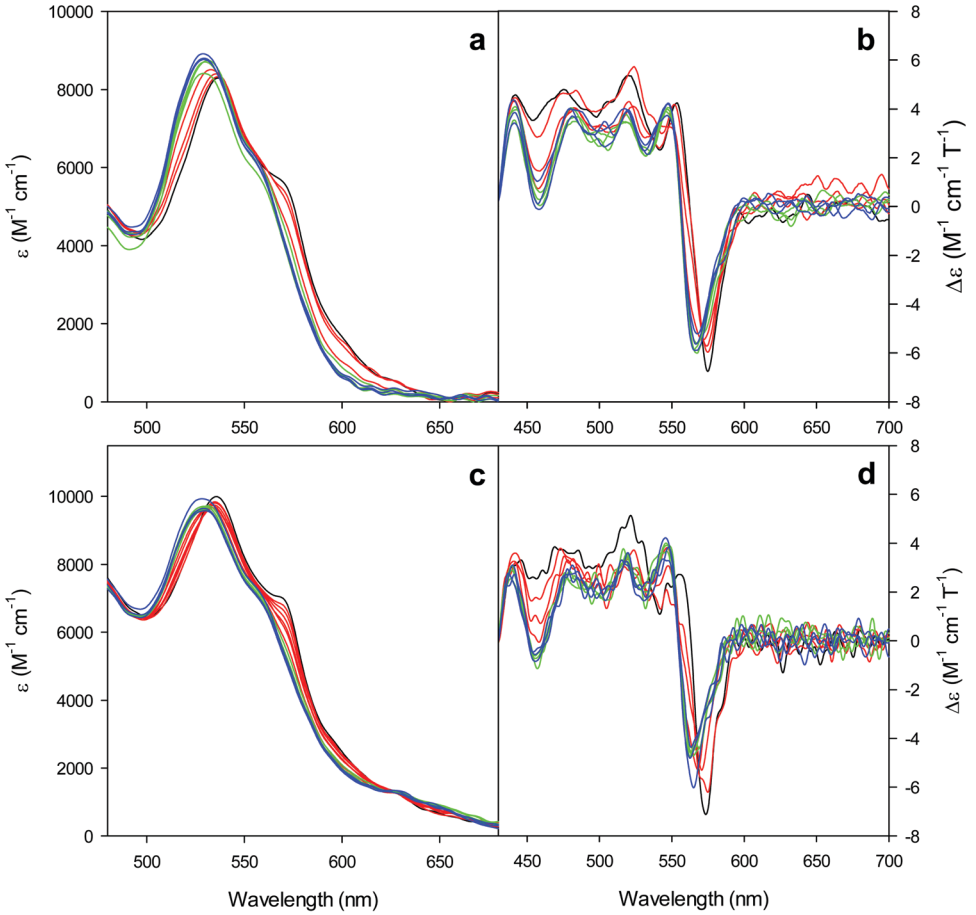

Fig. 3 Electronic absorption and MCD spectra in the visible region for the oxidized M80A (a and b) and M80AY67A (c and d) variants of *S. cerevisiae* iso-1 cytochrome *c* in 5 mM phosphate buffer at pH 7 in the presence of increasing urea concentration: 0 M (black); 1, 2, and 3 M (red); 4, 5, and 6 M (green); and 7, 8, and 9 M (blue).

Table 1 Wavelengths of the relevant spectral features of the UV-vis and MCD spectra for the M80A and M80A/Y67A variants of *Saccharomyces cerevisiae* iso-1 cytochrome *c* in 5 mM phosphate buffer pH 7 in the presence of different urea concentrations

		MCD						Absorption		
		Soret			Vis			Soret		
Species	[Urea]	Peak	Trough	Zerocross	Peak	Trough	Zerocross	Peak	2nd derivative	Vis
M80A	0	399	413	406	553	575, 542	562	404	406, 398(sh)	533, 565
	4	400	413	407	548	568, 532	556	406	407	528, 555
	9	400	413	407	547	568, 533	556	406	407, 398(sh)	528, 555
M80A/Y67A	0	398	412	405	555	573	566	405	407, 398(sh)	532, 562
	5	399	412	406	547	565	555	407	408	526, 555
	9	398	412	406	548	563	555	407	408	526, 555

up to 6 M in the working solution. A typical CV is shown in Fig. 6. Urea addition does not perturb the quasi-reversible electrochemical response but induces an anodic shift of $E^{\circ\prime}$ up to 0.024 V and 0.046 V for M80A and M80A/Y67A, respectively, at 6 M urea (Fig. 7 and Table 2). As no further $E^{\circ\prime}$ and spectroscopic changes occur at larger urea concentration, 6 M urea is taken as the condition that yields the fully unfolded ycc form. This urea-induced anodic shift is larger than that previously found for the same species immobilized on MUA–MU (0.011 V for M80A and 0.022 V for M80A/Y67A), which SERRS data showed to retain the His/OH^- axial heme iron coordination.[77] This fits with the urea-induced replacement of the axial hydroxide ion with an as yet unknown histidine residue to yield a bis-His axial ligand set. Indeed, the $E^{\circ\prime}$ values of both variants in 6 M urea are similar to those determined for urea unfolded wt ycc and its K72A/K73A/K79A mutant,[14] which were shown to possess His/His axial coordination.

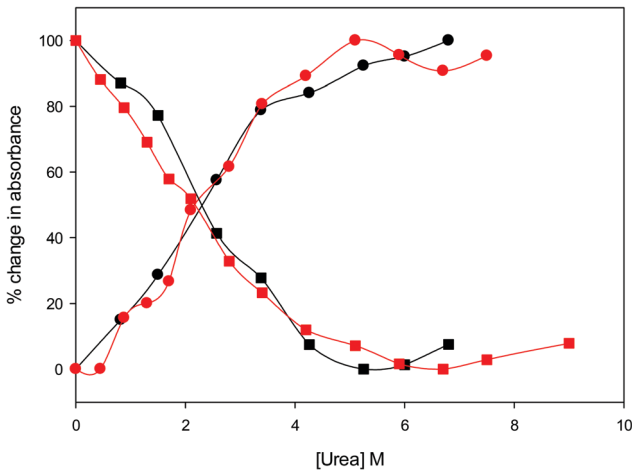

Fig. 4 Relative change in absorbance at 520 nm (circles) and 570 nm (squares) for the oxidized M80A (black) and M80AY67A (red) variants of *S. cerevisiae* iso-1 cytochrome *c* in 5 mM phosphate buffer at pH 7 in the presence of increasing urea concentration.

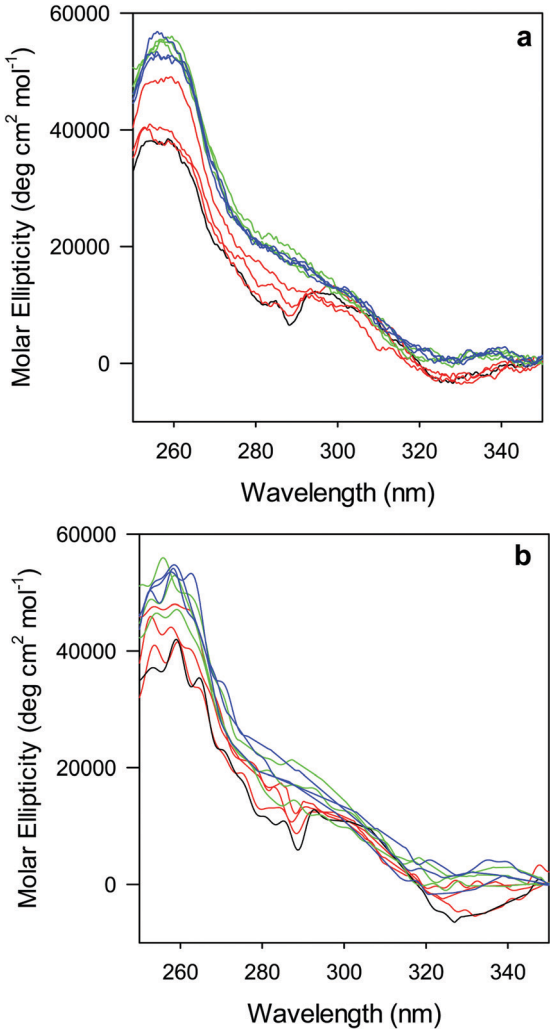

Fig. 5 Near UV CD spectra for the oxidized M80A (a) and M80AY67A (b) variants of *S. cerevisiae* iso-1 cytochrome *c* in 5 mM phosphate buffer at pH 7 in the presence of increasing urea concentration: 0 M (black); 1, 2, and 3 M (red); 4, 5, and 6 M (green); and 7, 8, and 9 M (blue).

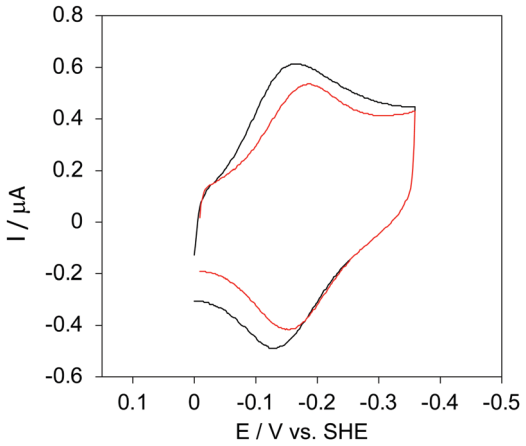

Fig. 6 Cyclic voltammograms for the M80A variant of yeast iso-1-cytochrome *c* in the presence of varying urea concentrations at pH 7.2 under diffusive conditions. 0 M urea (red) and 6 M urea (black). Working electrode: polycrystalline gold wire functionalized with 4-mercaptopyridine. Working solution: 10 mM phosphate buffer plus 100 mM sodium perchlorate, pH 7.2. T = 293 K. Sweep rate: 0.5 V s^{-1}. Similar CVs were obtained for the M80A/Y67A variant.

Thermodynamics of heme iron reduction

Valuable information on the mechanism of $E^{\circ\prime}_{\mathrm{Fe(III)/Fe(II)}}$ modulation in heme proteins has been obtained from the enthalpy $\left(\Delta H^{\circ\prime}_{\mathrm{rc}}\right)$ and entropy $\left(\Delta S^{\circ\prime}_{\mathrm{rc}}\right)$ changes accompanying the $Fe^{3+} \rightarrow Fe^{2+}$ reduction, determined by analyzing the temperature dependence of $E^{\circ\prime}$.[14,74–77,103,109–111,126–147] These thermodynamic data contain contributions from protein-based "intrinsic" factors $\left(\Delta H^{\circ\prime}_{\mathrm{rc(int)}};\ \Delta S^{\circ\prime}_{\mathrm{rc(int)}}\right)$ and solvent reorganization effects within the hydration sphere of the molecule $\left(\Delta H^{\circ\prime}_{\mathrm{rc(solv)}};\ \Delta S^{\circ\prime}_{\mathrm{rc(solv)}}\right)$.[33,74,75,103,126,128–133,135,138,139,145,146,148,149] The intrinsic enthalpic contribution depends on the donor properties of the axial heme ligands, the polarity and the electrostatics at the redox center, whereas the intrinsic entropic term is mainly controlled by oxidation-state dependent differences in the conformational degrees of freedom of the polypeptide chain.[74–77,98,99,103,126,128–133,135,137–139,144–149] For both variants, the $E^{\circ\prime}$ values increase linearly with increasing temperature with and without urea (Fig. 8a and b) and both display positive $\Delta S^{\circ\prime}_{\mathrm{rc}}$ and $\Delta H^{\circ\prime}_{\mathrm{rc}}$ values (Table 2). Hence, the enthalpic contribution disfavors Fe(III) reduction and is the main determinant of the negative $E^{\circ\prime}$ values, while Fe(III) reduction is favored entropically. In the absence of urea, the enthalpic stabilization of the oxidized heme in both mutants is largely the result of the strong electron donor character of the hydroxide ion and the mutation-induced increase in the exposure of the heme center to solvent resulting in greater solvation of the heme–protein interface.[76,77,98,99,147] The positive reduction entropy of both variants is consistent with the electrostatically driven increase in the disorder of the water molecules in the heme cavity due to the reduction of the net charge of the heme group (from 1+ to zero) upon Fe(III) reduction. A further contribution conceivably arises from the reduction-induced release

Table 2 Thermodynamic parameters for reduction of the M80A and M80A/Y67A variants of yeast iso-1-cytochrome *c* under freely diffusing conditions at varying urea concentration[a]

	M80A			M80AY67A		
[Urea] (M)	$E^{\circ\prime\,b}$ (V)	$\Delta H^{\circ\prime\,b}_{rc}$ (kJ mol^{-1})	$\Delta S^{\circ\prime\,b}_{rc}$ (J mol^{-1} K^{-1})	$E^{\circ\prime\,b}$ (V)	$\Delta H^{\circ\prime\,b}_{rc}$ (kJ mol^{-1})	$\Delta S^{\circ\prime\,b}_{rc}$ (J mol^{-1} K^{-1})
0	−0.170	41.8	85	−0.196	37.6	63
1	−0.165	37.5	72	−0.187	36.4	61
2	−0.157	34.3	64	−0.181	34.7	59
3	−0.155	32.3	59	−0.170	33.1	57
4	−0.152	29.8	51	−0.162	31.8	55
5	−0.147	28.0	46	−0.156	30.8	53
6	−0.146	26.9	43	−0.150	30.0	52

[a] Working electrode: polycrystalline gold electrode coated with a SAM of 4-mercapto-pyridine; working solution: 10 mM phosphate buffer plus 100 mM sodium perchlorate at pH 7.2. $E^{\circ\prime}$ is measured at T = 20 °C. [b] The average errors on $E^{\circ\prime}$, $\Delta H^{\circ\prime}_{rc}$ and $\Delta S^{\circ\prime}_{rc}$ are ±0.002 V, ±0.3 kJ mol^{-1} and ±2 J mol^{-1} K^{-1}, respectively.

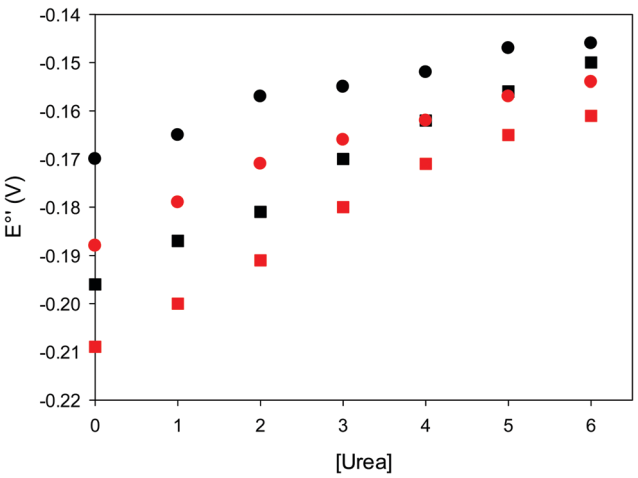

Fig. 7 Urea-induced changes in $E^{\circ\prime}$ for the M80A (circles) and M80AY67A (squares) variants of *S. cerevisiae* iso-1 cytochrome *c* at 5 °C (red) and 25 °C (black). Working electrode: polycrystalline gold wire functionalized with 4-mercapto-pyridine. 10 mM phosphate buffer plus 100 mM sodium perchlorate, pH 7.2.

of the axial hydroxide ligand.[76,77,98,99,147] Upon increasing the urea concentration, the $E^{\circ\prime}$ values increase while the reduction enthalpy and entropy values decrease. The following changes occur from 0 to 6 M urea for M80A and M80AY67A, respectively (Table 2): $\Delta E^{\circ\prime}$ = 0.024 and 0.046 V, $-\Delta\Delta H^{\circ\prime}_{rc}/F = +0.154$ and +0.079 V, $T\Delta\Delta S^{\circ\prime}_{rc}/F = -0.126$ and −0.033 V (at 293 K). Therefore, the change in the entropic term opposes but does not offset the enthalpic stabilization of the reduced form due to urea-induced unfolding and axial OH^- for His ligand swapping. Such a compensatory effect has been thoroughly described for several events in biomolecules and has been the subject of several theories and controversies.[18,20,74,76,77,133,146,150–164] For redox processes involving metal centers in proteins it can be considered the hallmark of the reduction-induced reorganization of the hydrogen bonding network within the hydration sphere of the molecule.[20,74,76,77,133,146,150–152,162,165–167] The linear $\Delta H^{\circ\prime}_{rc}$ *versus* $T\Delta S^{\circ\prime}_{rc}$ plots at 293 K for both mutants at different urea concentrations are reported in Fig. 9. The least-square fittings yield slopes of 1.23 and 2.40 and regression coefficients (r^2) of 0.999 and 0.995 for the M80A and M80A/Y67A mutants, respectively. As the changes in $\Delta H^{\circ\prime}_{rc}$ and $\Delta S^{\circ\prime}_{rc}$ arising from the reduction-induced reorganization of the H-bond network at the protein–solvent interface ($\Delta H^{\circ\prime}_{rc(solv)}$ and $\Delta S^{\circ\prime}_{rc(solv)}$) are fully compensative,[20,34,74,75,103,104,130–133,140,141,146–150] the absence of perfect compensation (*i.e.* slopes greater than one) indicates that, beside solvent reorganization effects, protein-based "intrinsic" factors significantly contribute to the urea-induced changes in the reduction thermodynamics. In particular, axial ligand swapping should lower the reduction enthalpy due to the slightly lower electron donor character of the His ligand compared to the hydroxide anion and to the resulting decreased exposure of the metal center to solvent. The less positive $\Delta S^{\circ\prime}_{rc}$ values of the His/His conformer fit with decreased solvent accessibility of the metal center, leading to a lower increase in the disorder of the water molecules in the heme cavity upon Fe(III) reduction.

The slopes of the compensation plots indicate that protein-based "intrinsic" factors exert a greater influence on the urea-induced changes in reduction enthalpy $[\Delta\Delta H^{\circ\prime}_{rc} = \Delta H^{\circ\prime}_{rc}(6\,\text{M urea}) - \Delta H^{\circ\prime}_{rc}(\text{no urea})]$ than the corresponding changes in reduction entropy $(\Delta\Delta S^{\circ\prime}_{rc})$ and that their effect is larger for the M80A/Y67A variant. This is also confirmed by the high compensation temperatures T_c featured by the M80A (359 K) and M80A/Y67A (695 K) mutants, which were calculated from the crossing point of the linear plots in Fig. 8. As the two mutants share the same axial heme coordination in both the folded (His/OH^-) and unfolded states (His/His), this behavior confirms that the alteration of the H-bonding network in the distal heme site due to the Tyr67 to Ala substitution generates specific mutation-induced changes in the electrostatics and polarity of the metal site of the folded protein, which apparently tend to disappear upon urea unfolding (Table 2).

Thermodynamics of urea-induced unfolding

The equation:

$$\Delta G^{\circ}_{u} = \Delta G^{\circ H_2O}_{u} - m \cdot [\text{urea}] \qquad (2)$$

puts in relation the free energies of unfolding in the presence of a denaturant (ΔG°_{u}) and at denaturant infinite dilution $(\Delta G^{\circ H_2O}_{u})$ for

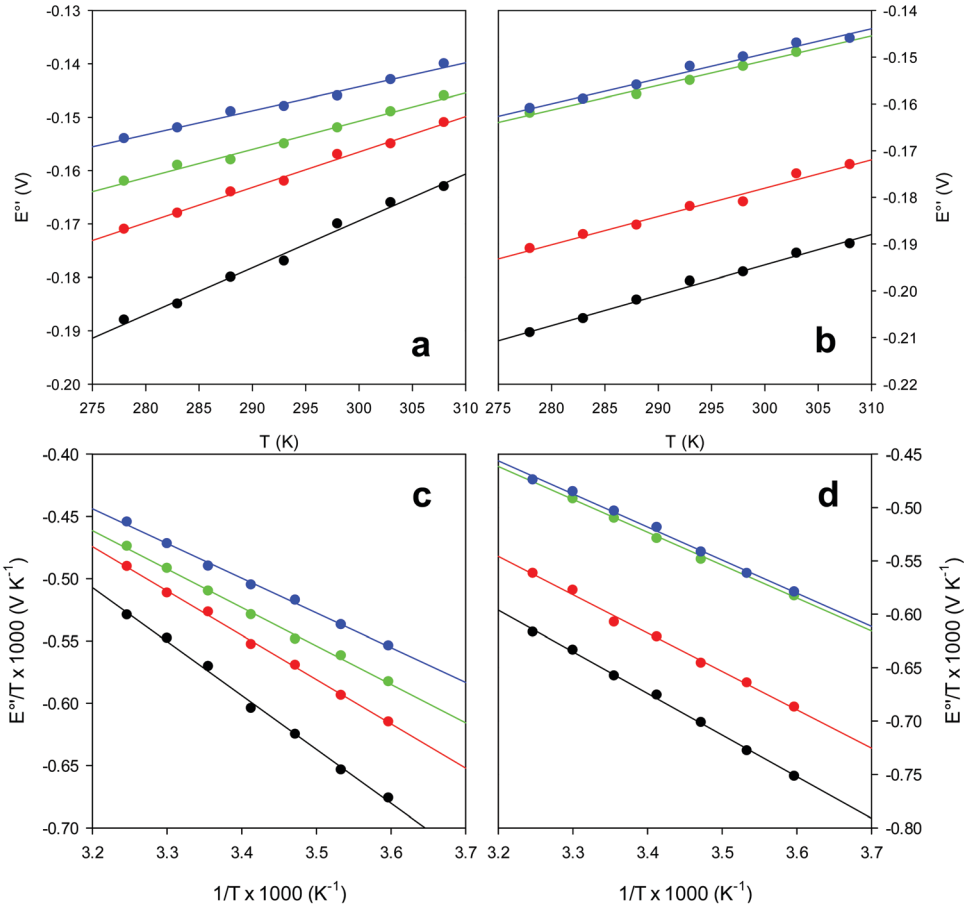

Fig. 8 Plot of $E^{\circ\prime}$ *versus* T and $E^{\circ\prime}/T$ *versus* $1/T$ for the M80A (a and c) and the M80A/Y67A (b and d) variants of yeast iso-1-cytochrome *c* in the presence of urea 0 M (black), 2 M (red), 4 M (green) and 6 M (blue), in 10 mM phosphate buffer plus 100 mM sodium perchlorate, pH 7.2. Solid lines are least-squares fits to the data points.

a two-state denaturation event, where m is a parameter proportional to the increase in the solvent-exposed surface area of the denatured state compared to the folded protein and provides an estimation of residual structure in the denatured state.[16,19,35,75,77,168,169] ΔG_u° can be calculated from the equilibrium constant, K_u, of the denaturation process at a given urea concentration:

$$\Delta G_u^\circ = -RT \cdot \ln K_u \quad (3)$$

where K_u is given by:

$$K_u = a_{\text{unfolded protein}}/a_{\text{folded protein}} \approx [\text{unfolded protein}]/[\text{folded protein}] \quad (4)$$

The concentration of folded and unfolded protein at each urea concentration was determined according to the following equations

$$[\text{unfolded protein}] = \alpha[\text{total protein concentration}] \quad (5)$$

$$[\text{folded protein}] = (1 - \alpha)[\text{total protein concentration}] \quad (6)$$

where α is the unfolding degree, calculated from (i) the measured $E^{\circ\prime}$ value at each urea concentration $\left(E_m^{\circ\prime}\right)$ and from the limit $E^{\circ\prime}$ values for the folded $\left(E_f^{\circ\prime}\right)$ and unfolded forms $\left(E_u^{\circ\prime}\right)$ measured at 0 and 6 M urea, respectively, and (ii) the intensity of the UV-vis and MCD spectra at selected wavelengths (520/570 nm and 575–573 nm, respectively) at each urea concentration (I_m) and for the folded (I_{mf}) and unfolded forms (I_{mu}) measured at 0 and 6 M urea, respectively, according to the following equations

$$\alpha = \frac{E_m^{\circ\prime} - E_f^{\circ\prime}}{E_u^{\circ\prime} - E_f^{\circ\prime}} \quad (7)$$

$$\alpha = \frac{I_m - I_f}{I_u - I_f} \quad (8)$$

The plots of ΔG_u° *vs.* urea concentration for both proteins are shown in Fig. 10. The $\Delta G_u^{\circ H_2O}$ and m values obtained from the intercept and the slope of the least-squares linear fit of the data points to eqn (2), respectively, are listed in Table 3, along with the data obtained previously for wt ycc and its K72A/K73A/K79A and K72A/K73H/K79A mutants.[14,75] The variable-temperature voltammetric measurements carried out at different urea concentrations allow the $\Delta G_u^{\circ H_2O}$ and m values from 5 to 35 °C to be determined. Both terms slightly decrease with increasing temperature (Table 3). The $\Delta G_u^{\circ H_2O}$ values for both variants are

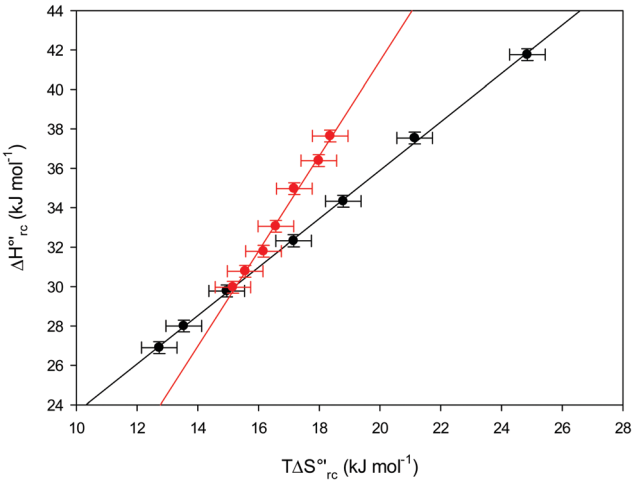

Fig. 9 Enthalpy–entropy compensation plots for the reduction thermodynamics of the M80A (black) and the M80A/Y67A (red) variants of yeast iso-1-cytochrome *c*, in the presence of varying urea concentrations: 0 M, 1 M, 2 M, 3 M, 4 M, 5 M and 6 M in 10 mM phosphate buffer plus 100 mM sodium perchlorate, pH 7.2. Solid lines are least-squares fits to the data points. T = 293 K. Error bars were calculated from the average errors on $\Delta H^{\circ\prime}$ and $\Delta S^{\circ\prime}_{rc}$ reported in Table 2.

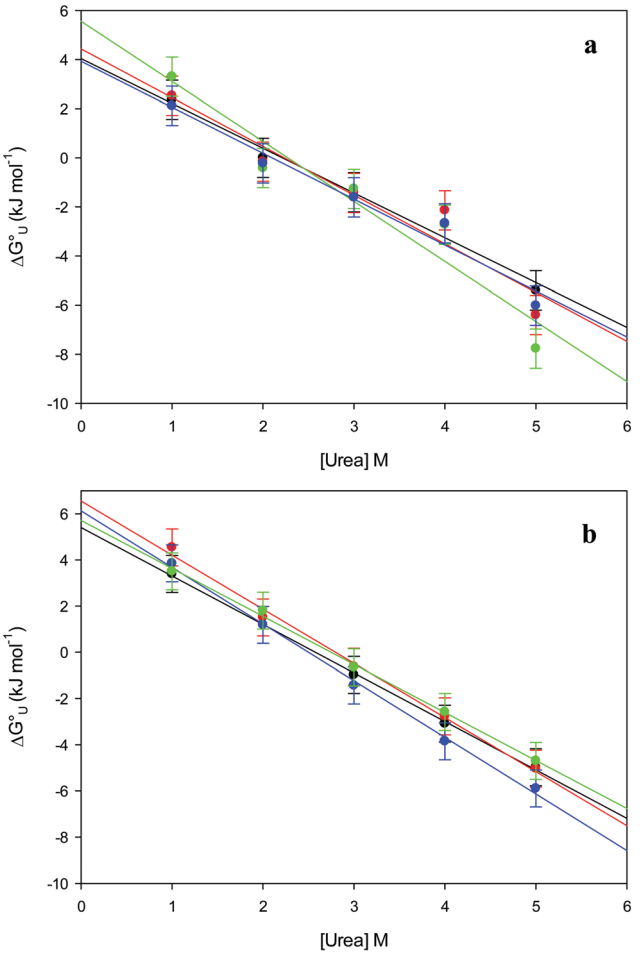

Fig. 10 Plots of ΔG°_{u} *versus* molar urea concentration for the M80A (a) and the M80A/Y67A (b) variants of yeast iso-1-cytochrome *c* in 10 mM phosphate buffer plus 100 mM sodium perchlorate, pH 7.2. T = 278 K (black), 288 K (red), 298 K (green) and 308 K (blue). According to eqn (2), $\Delta G^{\circ H_2O}_{u}$ and m are obtained from the intercept and the slope of the least-squares linear fit of the data points, respectively.

significantly lower than those for the species showing intact Met/His coordination, as previously observed for the same species immobilized on a MUA/MU SAM at the same T (5 °C).[77] This indicates that the axial Fe–(S)Met bond plays a significant role in determining the stability of cytochrome *c* against chemical denaturation, as its removal invariably "relaxes" the 3D structure of the protein and facilitates unfolding. The additional Y67A mutation disfavors to some extent protein unfolding, since the $\Delta G^{\circ H_2O}_{u}$ values for the M80A/Y67A variant are slightly larger (0.7–0.8 kJ mol^{-1}) than for M80A. Hence, the alteration of the H-bonding network that stabilizes the heme crevice due to the Y67A mutation[85–96] results in a larger inherent thermodynamic stability of the protein. This finding is rather surprising, since Tyr67 mutation would be expected to facilitate unfolding, but this conflict is only apparent because the difference in free energy of unfolding between the single and double mutant turns out to be an entropic effect, as discussed below.

The M80A and M80AY67A variants feature quite similar m values (Table 3) throughout the temperature range investigated. We note that at 5 °C the m values are comparable to those for the Met/His-ligated species (wt and variants to surface lysines), but lower than that of the K72A/K73H/K79A variant. Therefore, it appears that at low temperature neither removal of the axial Fe–(S)Met bond, also coupled to alteration of the H-bonding network stabilizing the heme crevice (M80A/Y67A), nor deletion of surface charges (K72A/K73A/K79A) significantly influences the structural impact of urea on the overall ycc folding, which instead is affected by insertion of a new potential axial ligand (K72A/K73H/K79A). On the contrary, at 25 °C the m values for M80A and M80AY67A are much lower compared to the wt (Table 3), indicative of a smaller increase in the solvent-exposed surface area. However, this effect is not the result of less pronounced protein unfolding as the near-UV CD spectra (Fig. 5) indicate that the variants and wt both undergo disruption of the tight packing of the core residues.[84,90,122] A possible role in this effect is played by the different urea-induced axial ligand swapping occurring in the variants compared to the wt.

The enthalpy and entropy changes associated with the unfolding process calculated using the van't Hoff equation from the temperature dependence of $\Delta G^{\circ H_2O}_{u}$ are positive for both species (Fig. 11 and Table 4). Hence, the urea-induced denaturation realizes an entropic gain but is disfavored on enthalpic grounds. The enthalpy change is the main determinant of the positive $\Delta G^{\circ H_2O}_{u}$ values (Fig. 12 and Table 4).

As suggested previously,[77] the enthalpic cost of urea unfolding results from the balance of bond breaking and formation, involving heme axial ligand swapping and intramolecular and intermolecular protein–solvent van der Waals interactions and H-bonding, associated with urea intrusion into the tertiary structure followed by hydration and loss of the native structure.[170] The positive unfolding entropy possibly results

Table 3 $\Delta G_u^{\circ H_2O}$ and m values at different temperatures for the urea-induced unfolding of the M80A and M80AY67A variants of yeast iso-1-cytochrome *c*

Protein	T (°C)	$\Delta G_u^{\circ H_2O}{}_a$ (kJ mol^{-1})	m^a (kJ mol^{-1} M^{-1})
M80A$_{sol}$	5	5.98^b	2.64^b
	10	5.65^b	2.59^b
	15	5.44^b	2.38^b
	20	5.33^b	2.47^b
	25	5.20^b	2.15^b
	30	4.42^b	1.93^b
	35	4.60^b	2.07^b
	25	6.16^c	2.51^c
M80A$_{ads}$	5	4.9^d	2.16^d
	25	0.95^d	1.52^d
M80AY67A$_{sol}$	5	6.72^b	2.64^b
	10	6.31^b	2.39^b
	15	6.27^b	2.03^b
	20	6.13^b	1.81^b
	25	6.05^b	2.10^b
	30	5.92^b	1.87^b
	35	5.80^b	2.13^b
	25	6.87^c	2.98^c
M80AY67A$_{ads}$	5	6.6^d	2.52^d
	25	3.75^d	1.71^d
K72A/K73H/K79A$_{sol}$	5	12.7^e	4.2^e
K72A/K73A/K79A$_{sol}$	5	8.1^f	2.3^f
wt$_{sol}$	5	7.6^f	1.9^f
	25	20.8^g	6.90^g
K73H	25	15.2^g	5.1^g

^{a} The errors on $\Delta G_u^{\circ H_2O}$ and m are ±0.80 kJ mol^{-1} and ±10% (relative error), respectively. ^{b} From voltammetric experiments carried out in 10 mM phosphate buffer plus 100 mM sodium perchlorate at pH 7.2. ^{c} Average values calculated from the changes in the UV-vis and MCD spectra at selected wavelengths (520/570 nm and 575–573 nm, respectively) observed in the presence of an increasing concentration of urea in 5 mM phosphate buffer pH 7. ^{d} From ref. 77. ^{e} From ref. 75. ^{f} Calculated form data in ref. 14. ^{g} From ref. 35.

from the urea-induced weakening of the structural constraints and intramolecular bonding interactions in the secondary and tertiary structure of the polypeptide chain, which results in increased molecular accessible states and degrees of freedom. Likewise, elimination of constrained water assemblies on the protein surface due to hydrophobic hydration upon displacement by the larger urea molecules possibly contributes to the entropy gain.[77,171] The opposite contributions of the enthalpic and entropic terms to $\Delta G_u^{\circ H_2O}$ (H–S compensation) (Table 4 and Fig. 12) confirm that changes in the hydrogen bonding network in the hydration sphere of the protein upon unfolding strongly affect the thermodynamics of the denaturation process. The increase of $\Delta G_u^{\circ H_2O}$ for M80A/Y67A compared to M80A is entropy-driven (Table 4 and Scheme 1). The similarity of the urea-induced changes in the spectroscopic properties of the two mutants suggests that such an effect has more to do with the increased hydrophobicity of the heme cavity following the substitution of a hydrophilic Tyr with a hydrophobic Ala residue

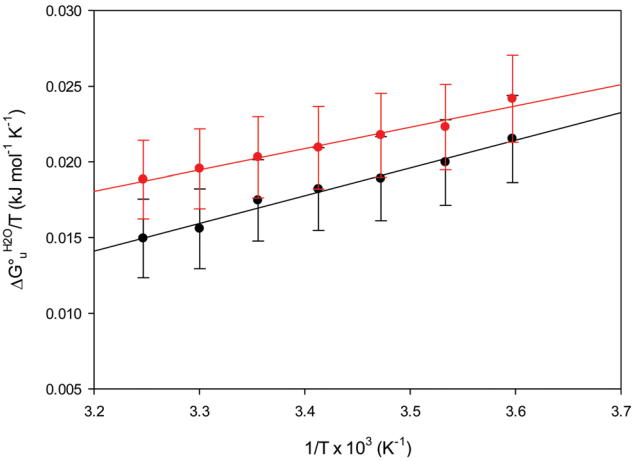

Fig. 11 vant'Hoff plots for the urea-induced unfolding of the M80A (black) and the M80A/Y67A (red) variants of yeast iso-1-cytochrome *c* in 10 mM phosphate buffer plus 10 mM sodium perchlorate, pH 7.2. Solid lines are least-squares fits to the data points.

than to mutation-specific differences in the structural changes upon urea-induced unfolding.

Solution *versus* immobilized state

A comparison of the present data with those obtained previously for the same mutants adsorbed electrostatically on a MUA/MU SAM allows examination of how the thermodynamics of urea-induced unfolding are affected by protein adsorption. The $\Delta G_u^{\circ H_2O}$ values for the solution variants are larger with respect to those for the same electrode-immobilized species, especially at 25 °C. Therefore, immobilization favors the chemically-induced protein unfolding (Table 4 and Scheme 1). Both proteins feature much less positive $\Delta H_u^{\circ H_2O}$ and $\Delta S_u^{\circ H_2O}$ values in freely diffusing conditions than in the immobilized state (Table 4 and Scheme 1). The changes in the unfolding enthalpy and entropy are much larger than the changes in the unfolding free energy (Scheme 1). Once again, this H–S compensation indicates that differences in solvent reorganization effects accompanying denaturation of the protein under freely diffusing conditions or subjected to motional restriction are the main factor responsible for the differences in $\Delta H_u^{\circ H_2O}$ and $\Delta S_u^{\circ H_2O}$. This balance however changes with temperature. In particular, at 5 °C the enthalpy/entropy compensation is almost perfect, resulting in very limited (M80A) or negligible (M80AY67A) free energy differences, but decreases with increasing temperature, leading to sizeable changes in the $\Delta G_u^{\circ H_2O}$ values for immobilized and freely diffusing proteins at room temperature (Table 3). Analogously, Δm [=m(ads) − m(sol)] becomes more negative with increasing temperature. At 25 °C, electrostatic adsorption on MUA/MU induces a progressive lowering of the inherent thermodynamic stability of the three-dimensional structure of both proteins and reduces the increase in the solvent-exposed surface area of the denatured state compared to the folded protein. It is tempting to speculate that a non-negligible contribution to the higher $\Delta G_u^{\circ H_2O}$ values of the freely diffusing species at room

Table 4 Thermodynamic parameters of urea-induced unfolding for yeast iso-1-cytochrome *c* and variants in solution and in the immobilized state

Protein	T	$\Delta G_u^{\circ H_2O a}$ (kJ mol^{-1})	$\Delta H_u^{\circ H_2O a}$ (kJ mol^{-1})	$\Delta S_u^{\circ H_2O a}$ (J K^{-1} mol^{-1})	$T\Delta S_u^{\circ H_2O a,b}$ (kJ mol^{-1})	m^a (kJ mol^{-1} M^{-1})
M80A in solution[c]	5	6.0	18.3	44.4	12	2.64
M80AY67A in solution[c]	5	6.7	14.1	27.1	8	2.64
M80A immobilized[d]	5	4.9	58.5	191.5	53	2.19
M80AY67A immobilized[d]	5	6.6	46.6	142.4	40	2.61
wt immobilized[d,e]	5	13.4	91.8	286.6	77	3.24
K72A/K73A/K79A immobilized[d,e]	5	11.3	69.9	209.3	58	2.95

[a] The average errors on $\Delta G_u^{\circ H_2O}$, $\Delta H_u^{\circ H_2O}$, $\Delta S_u^{\circ H_2O}$ and m are ±0.8 kJ mol^{-1}, ±8% (relative error), ±10% (relative error) and ±10% (relative error), respectively. [b] At 5 °C. [c] Present work, freely diffusing species in 10 mM phosphate buffer plus 100 mM sodium perchlorate, pH 7.2. [d] Protein adsorbed on a polycrystalline gold electrode coated with a SAM of MUA/MU, from ref. 77. [e] Values calculated from data in ref. 74.

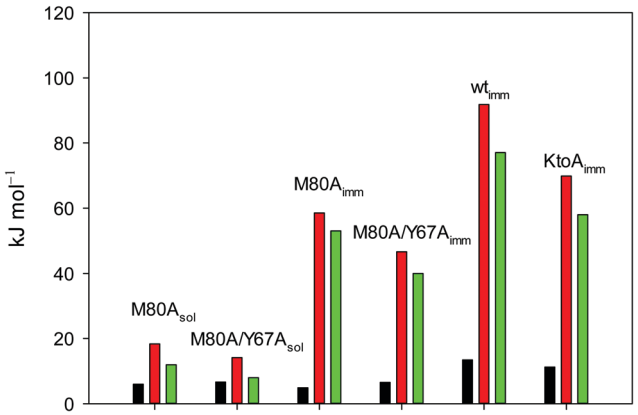

Fig. 12 Histograms depicting the thermodynamic parameters of urea-induced unfolding for yeast iso-1-cytochrome *c* and its variants in solution and in the immobilized state reported in Table 4. Black, red and green bars correspond to $\Delta G_u^{\circ H_2O}$, $\Delta H_u^{\circ H_2O}$ and T (5 °C)·$\Delta S_u^{\circ H_2O}$ values, respectively.

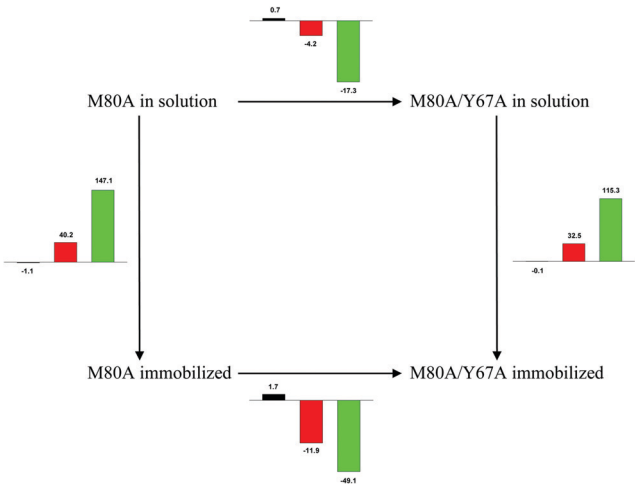

Scheme 1 Cycle summarizing (i) the effects of the Y67A mutation on the unfolding thermodynamics of the M80A variant of yeast iso-1-cytochrome *c* in freely diffusing conditions (upper line) and immobilized on a MUA/MU SAM (bottom line) and (ii) the effect of immobilization on a MUA/MU SAM on the unfolding thermodynamics of the M80A and M80A/Y67A variants of yeast iso-1-cytochrome *c* (left and right column, respectively). $\Delta\Delta G_u^{\circ H_2O}$ (kJ mol^{-1}, black column), $\Delta\Delta H_u^{\circ H_2O}$ (kJ mol^{-1}, red column) and $\Delta\Delta S_u^{\circ H_2O}$ (J K^{-1} mol^{-1}, green column) were calculated form the data reported in Table 4.

temperature results from the urea-induced replacement of the axial OH^- by an endogenous histidine, which does not occur upon protein immobilization.

The negative Δm [=m(ads) − m(sol)] values for both the M80A and M80AY67A variants indicate that the urea-induced increase in the solvent-exposed surface area is less pronounced for the immobilized species. Although this effect does not match intuitively with the larger thermodynamic tendency of the latter species to unfold (lower $\Delta G_u^{\circ H_2O}$ values), it fits well with the hypothesis that both mutants undergo non-negligible unfolding upon adsorption on a MUA/MU SAM, which lowers the effects of structure opening to solvent due to eventual urea unfolding, thereby preventing the coordination of a second His ligand at high urea concentrations.[77]

Conclusions

Partial protein unfolding due to a chemical stimulus, in general represented by the binding of an effector molecule or adsorption onto a supramolecular assembly (*e.g.* cell or organelle membrane), is a strategy widely employed by biological systems to transmit a chemical message or trigger a biochemical event. Cytochrome *c* participates in this kind of mechanisms. In fact, upon binding to cardiolipin, a component of the inner mitochondrial membrane (IMM), cytc is subjected to a structural change that results in oxidative reactions leading to its release from the mitochondrion to the cytosol whereby it activates caspases that initiate the cell apoptotic cascade. Here we have presented evidence that at room (or physiological) temperature the susceptibility to unfolding of ycc – represented by the free energy of unfolding at denaturant infinite dilution $\Delta G_u^{\circ H_2O}$ – is affected by the motional regime of the protein, namely it differs depending on whether the protein is freely diffusing or subjected to a motional restriction due to the interaction with a molecular construct. In particular, electrostatic adsorption onto a negatively charged molecular surface (a MUA/MU SAM, which would mimic the negatively charged phospholipidic inner mitochondrial membrane) renders ycc more susceptible to chemical unfolding compared to the solution state. This finding has physiological relevance related to the cytochrome *c* interaction with cardiolipin at the IMM. Such motional state-dependent behavior results in different molecular events involving the change in axial ligands of the heme iron and different unfolding-induced changes in the hydrogen bonding network

within the hydration sphere of the molecule. As we have also found previously that the unfolding behavior of immobilized ycc changes with the nature of the adsorbing construct,[76,77] it is apparent how, from a more general perspective, the motional properties of the protein and the nature of the adsorbing surface constitute additional means that Nature can exploit to modulate protein unfolding and the eventual molecular response.[5,13,31]

Funding information

This work was supported by the University of Modena and Reggio Emilia FAR 2019 funding program.

Conflicts of interest

There are no conflicts of interest to declare.

References

1 D. Alvarez-Paggi, L. Hannibal, M. A. Castro, S. Oviedo-Rouco, V. Demicheli, V. Tórtora, F. Tomasina, R. Radi and D. H. Murgida, *Chem. Rev.*, 2017, **117**, 13382–13460.
2 S. Zaidi, M. I. Hassan, A. Islam and F. Ahmad, *Cell. Mol. Life Sci.*, 2014, **71**, 229–255.
3 I. Bertini, G. Cavallaro and A. Rosato, *Chem. Rev.*, 2006, **106**, 90–115.
4 M. Hüttemann, P. Pecina, M. Rainbolt, T. H. Sanderson, V. E. Kagan, L. Samavati, J. W. Doan and I. Lee, *Mitochondrion*, 2011, **11**, 369–381.
5 R. Schweitzer-Stenner, *Biophys. Rev.*, 2018, **10**, 1151–1185.
6 G. W. Moore and G. R. Pettigrew, *Cytochromes c. Evolutionary, Structural, and Physicochemical Aspects*, Springer-Verlag, Berlin, Germany, 1990.
7 *Cytochrome c – A Multidisciplinary Approach*, ed. A. G. Scott and R. A. Mauk, University Science Books, Sausalito, CA, 1996.
8 G. Battistuzzi, M. Borsari, L. Loschi, A. Martinelli and M. Sola, *Biochemistry*, 1999, **38**, 7900–7907.
9 G. Battistuzzi, M. Borsari, G. Rossi and M. Sola, *Inorg. Chim. Acta*, 1998, **272**, 168–175.
10 G. Battistuzzi, M. Borsari, A. Ranieri and M. Sola, *Arch. Biochem. Biophys.*, 2002, **404**, 227–233.
11 G. Battistuzzi, M. Borsari and M. Sola, *Eur. J. Inorg. Chem.*, 2001, 2989.
12 G. Battistuzzi, M. Borsari, F. De Rienzo, G. Di Rocco, A. Ranieri and M. Sola, *Biochemistry*, 2007, **46**, 1694–1702.
13 A. Paradisi, M. Bellei, L. Paltrinieri, C. A. Bortolotti, G. Di Rocco, A. Ranieri, M. Borsari, M. Sola and G. Battistuzzi, *JBIC, J. Biol. Inorg. Chem.*, 2020, **25**, 467–487.
14 S. Monari, A. Ranieri, G. Di Rocco, G. van der Zwan, S. Peressini, C. Tavagnacco, D. Millo and M. Borsari, *J. Appl. Electrochem.*, 2009, **39**, 2181–2190.
15 N. A. Belikova, Y. A. Vladimirov, A. N. Osipov, A. A. Kapralov, V. A. Tyurin, M. V. Potapovich, L. V. Basova, J. Peterson, I. V. Kurnikov and V. E. Kagan, *Biochemistry*, 2006, **45**, 4998–5009.
16 S.-R. Yeh, S. Han and D. L. Rousseau, *Acc. Chem. Res.*, 1998, **31**, 727–736.
17 S. W. Englander, T. R. Sosnick, L. C. Mayne, M. Shtilerman, P. X. Qi and Y. Bai, *Acc. Chem. Res.*, 1998, **31**, 737–744.
18 L. Hoang, S. Bédard, M. M. G. Krishna, Y. Lin and S. W. Englander, *Proc. Natl. Acad. Sci. U. S. A.*, 2002, **99**, 12173–12178.
19 S.-R. Yeh and D. L. Rousseau, *Nat. Struct. Biol.*, 1998, **5**, 222–228.
20 M. Fedurco, J. Augustynski, C. Indiani, G. Smulevich, M. Antalík, M. Bánó, E. Sedlák, M. C. Glascock and J. H. Dawson, *J. Am. Chem. Soc.*, 2005, **127**, 7638–7646.
21 M. Fedurco, J. Augustynski, C. Indiani, G. Smulevich, M. Antalík, M. Bánó, E. Sedlák, M. C. Glascock and J. H. Dawson, *Biochim. Biophys. Acta, Proteins Proteomics*, 2004, **1703**, 31–41.
22 S. Baddam and B. E. Bowler, *Biochemistry*, 2005, **44**, 14956–14968.
23 R. Schweitzer-Stenner, *New J. Sci.*, 2014, **2014**, 1–28.
24 N. J. O'Reilly and E. Magner, *Langmuir*, 2005, **21**, 1009–1014.
25 S. Crilly and E. Magner, *Chem. Commun.*, 2009, 535–537.
26 G. Battistuzzi, M. Borsari and M. Sola, *Trends Inorg. Chem.*, 1996, **4**, 1–8.
27 G. Battistuzzi, M. Borsari, D. Dallari, I. Lancellotti and M. Sola, *Eur. J. Biochem.*, 1996, **241**, 208–214.
28 A. Díaz-Quintana, G. Pérez-Mejías, A. Guerra-Castellano, M. A. De la Rosa and I. Díaz-Moreno, *Oxid. Med. Cell. Longev.*, 2020, **2020**, 1–20.
29 S. Oellerich, H. Wackerbarth and P. Hildebrandt, *J. Phys. Chem. B*, 2002, **106**, 6566–6580.
30 P. Ascenzi, M. Coletta, M. T. Wilson, L. Fiorucci, M. Marino, F. Polticelli, F. Sinibaldi and R. Santucci, *IUBMB Life*, 2015, **67**, 98–109.
31 J. Muenzner and E. V. Pletneva, *Chem. Phys. Lipids*, 2014, **179**, 57–63.
32 A. Ranieri, D. Millo, G. Di Rocco, G. Battistuzzi, C. A. Bortolotti, M. Borsari and M. Sola, *JBIC, J. Biol. Inorg. Chem.*, 2015, **20**, 531–540, DOI: 10.1007/s00775-015-1238-6.
33 A. Ranieri, G. Di Rocco, D. Millo, G. Battistuzzi, C. A. Bortolotti, L. Lancellotti, M. Borsari and M. Sola, *Electrochim. Acta*, 2015, **176**, 1019–1028.
34 A. Ranieri, G. Battistuzzi, M. Borsari, C. A. Bortolotti, G. Di Rocco, S. Monari and M. Sola, *Electrochem. Commun.*, 2012, **14**, 29–31.
35 S. Godbole, A. Dong, K. Garbin and B. E. Bowler, *Biochemistry*, 1997, **36**, 119–126.
36 S. Baddam and B. E. Bowler, *Biochemistry*, 2006, **45**, 4611–4619.
37 M. G. Duncan, M. D. Williams and B. E. Bowler, *Protein Sci.*, 2009, **18**, 1155–1164, DOI: 10.1002/pro.120.
38 M. M. Elmer-Dixon and B. E. Bowler, *Biochemistry*, 2018, **57**, 5683–5695.
39 G. Battistuzzi, M. Borsari, A. Ranieri and M. Sola, *J. Biol. Inorg. Chem.*, 2004, **9**, 781–787.
40 V. E. Kagan, H. A. Bayir, N. A. Belikova, O. Kapralov, Y. Y. Tyurina, V. A. Tyurin, J. Jiang, D. A. Stoyanovsky,

P. Wipf, P. M. Kochanek, J. S. Greenberger, B. Pitt, A. A. Shvedova and G. Borisenko, *Free Radicals Biol. Med.*, 2009, **46**, 1439–1453.
41 M. M. Cherney and B. E. Bowler, *Coord. Chem. Rev.*, 2011, **255**, 664–677.
42 B. Milorey, R. Schweitzer-Stenner, R. Kurbaj and D. Malyshka, *ACS Omega*, 2019, **4**, 1386–1400.
43 L. Hannibal, F. Tomasina, D. A. Capdevila, V. Demicheli, V. Tórtora, D. Alvarez-Paggi, R. Jemmerson, D. H. Murgida and R. Radi, *Biochemistry*, 2016, **55**, 407–428.
44 D. A. Capdevila, S. Oviedo Rouco, F. Tomasina, V. Tortora, V. Demicheli, R. Radi and D. H. Murgida, *Biochemistry*, 2015, **54**, 7491–7504.
45 L. A. Pandiscia and R. Schweitzer-Stenner, *J. Phys. Chem. B*, 2015, **119**, 12846–12859.
46 L. Pandiscia and R. Schweitzer-Stenner, *Biophys. J.*, 2015, **106**, 517a.
47 M. Li, A. Mandal, V. A. Tyurin, M. DeLucia, J. Ahn, V. E. Kagan and P. C. A. van der Wel, *Structure*, 2019, 1–11.
48 D. Mohammadyani, N. Yanamala, A. K. Samhan-Arias, A. A. Kapralov, G. Stepanov, N. Nuar, J. Planas-Iglesias, N. Sanghera, V. E. Kagan and J. Klein-Seetharaman, *Biochim. Biophys. Acta, Biomembr.*, 2018, **1860**, 1057–1068.
49 B. Milorey, D. Malyshka and R. Schweitzer-Stenner, *J. Phys. Chem. Lett.*, 2017, **8**, 1993–1998.
50 J. M. Bradley, G. Silkstone, M. T. Wilson, M. R. Cheesman and J. N. Butt, *J. Am. Chem. Soc.*, 2011, **133**, 19676–19679.
51 B. S. Rajagopal, G. G. Silkstone, P. Nicholls, M. T. Wilson and J. A. R. Worrall, *Biochim. Biophys. Acta, Bioenerg.*, 2012, **1817**, 780–791.
52 J. Hanske, J. R. Toffey, A. M. Morenz, A. J. Bonilla, K. H. Schiavoni and E. V. Pletneva, *Proc. Natl. Acad. Sci. U. S. A.*, 2011, **109**, 125–130.
53 Y. Hong, J. Muenzner, S. K. Grimm and E. V. Pletneva, *J. Am. Chem. Soc.*, 2012, **134**, 18713–18723.
54 C. Kawai, J. C. Ferreira, M. S. Baptista and I. L. Nantes, *J. Phys. Chem. B*, 2014, **118**, 11863–11872.
55 J. Muenzner, J. R. Toffey, Y. Hong and E. V. Pletneva, *J. Phys. Chem. B*, 2013, **117**, 12878–12886.
56 E. K. J. Tuominen, C. J. A. Wallace and P. K. J. Kinnunen, *J. Biol. Chem.*, 2002, **277**, 8822–8826.
57 E. Kalanxhi and C. J. A. Wallace, *Biochem. J.*, 2007, **407**, 179–187.
58 F. Sinibaldi, L. Fiorucci, A. Patriarca, R. Lauceri, T. Ferri, M. Coletta and R. Santucci, *Biochemistry*, 2008, **47**, 6928–6935.
59 F. Sinibaldi, B. D. Howes, M. C. Piro, F. Polticelli, C. Bombelli, T. Ferri, M. Coletta, G. Smulevich and R. Santucci, *J. Biol. Inorg. Chem.*, 2010, **15**, 689–700.
60 F. Sinibaldi, E. Droghetti, F. Polticelli, M. C. Piro, D. Di Pierro, T. Ferri, G. Smulevich and R. Santucci, *J. Inorg. Biochem.*, 2011, **105**, 1365–1372.
61 M. C. Piro, R. Santucci, E. Droghetti, F. Sinibaldi, L. Fiorucci, M. Coletta, D. Di Pierro, B. D. Howes, F. Polticelli and G. Smulevich, *Biochemistry*, 2013, **52**, 4578–4588.
62 L. Milazzo, L. Tognaccini, B. D. Howes, F. Sinibaldi, M. C. Piro, M. Fittipaldi, M. C. Baratto, R. Pogni, R. Santucci and G. Smulevich, *Biochemistry*, 2017, **56**, 1887–1898.
63 G. Silkstone, S. M. Kapetanaki, I. Husu, M. H. Vos and M. T. Wilson, *Biochemistry*, 2012, **51**, 6760–6766.
64 I. Husu, S. Kapetanaki, G. Silkstone, U. Liebl, M. T. Wilson and M. Vos, *Biophys. J.*, 2010, **98**, 631a.
65 S. M. Kapetanaki, G. Silkstone, I. Husu, U. Liebl, M. T. Wilson and M. H. Vos, *Biochemistry*, 2009, **48**, 1613–1619.
66 M. M. Elmer-Dixon and B. E. Bowler, *Biochemistry*, 2017, **56**, 4830–4839.
67 L. A. Pandiscia and R. Schweitzer-Stenner, *Chem. Commun.*, 2014, **50**, 3674–3676.
68 F. Sinibaldi, L. Milazzo, B. D. Howes, M. C. Piro, L. Fiorucci, F. Polticelli, P. Ascenzi, M. Coletta, G. Smulevich and R. Santucci, *JBIC, J. Biol. Inorg. Chem.*, 2017, **22**, 19–29.
69 P. Ascenzi, D. Sbardella, F. Sinibaldi, R. Santucci and M. Coletta, *JBIC, J. Biol. Inorg. Chem.*, 2016, **21**, 421–432.
70 L. Zeng, L. Wu, L. Liu and X. Jiang, *Anal. Chem.*, 2016, **88**, 11727–11733.
71 S. S. Paul, P. Sil, S. Haldar, S. Mitra and K. Chattopadhyay, *J. Biol. Chem.*, 2015, **290**, 14476–14490.
72 L. C. Godoy, C. Muñoz-Pinedo, L. Castro, S. Cardaci, C. M. Schonhoff, M. King, V. Tórtora, M. Marín, Q. Miao, J. F. Jiang, A. Kapralov, R. Jemmerson, G. G. Silkstone, J. N. Patel, J. E. Evans, M. T. Wilson, D. R. Green, V. E. Kagan, R. Radi and J. B. Mannick, *Proc. Natl. Acad. Sci. U. S. A.*, 2009, **106**, 2653–2658.
73 M. Abe, R. Niibayashi, S. Koubori, I. Moriyama and H. Miyoshi, *Biochemistry*, 2011, **50**, 8383–8391.
74 S. Monari, D. Millo, A. Ranieri, G. Di Rocco, G. van der Zwan, C. Gooijer, S. Peressini, C. Tavagnacco, P. Hildebrandt and M. Borsari, *JBIC, J. Biol. Inorg. Chem.*, 2010, **15**, 1233–1242.
75 A. Ranieri, C. A. Bortolotti, G. Battistuzzi, M. Borsari, L. Paltrinieri, G. Di Rocco and M. Sola, *Metallomics*, 2014, **6**, 874–884.
76 L. Lancellotti, M. Borsari, A. Bonifacio, C. A. Bortolotti, G. Di Rocco, S. Casalini, A. Ranieri, G. Battistuzzi and M. Sola, *Bioelectrochemistry*, 2020, **136**, 107628, DOI: 10.1016/j.bioelechem.2020.107628.
77 L. Lancellotti, M. Borsari, M. Bellei, A. Bonifacio, C. A. Bortolotti, G. Di Rocco, A. Ranieri, M. Sola and G. Battistuzzi, submitted.
78 M. M. G. Krishna, Y. Lin, J. N. Rumbley and S. W. Englander, *J. Mol. Biol.*, 2003, **331**, 29–36.
79 L. Hoang, H. Maity, M. M. G. Krishna, Y. Lin and S. W. Englander, *J. Mol. Biol.*, 2003, **331**, 37–43.
80 E. Droghetti, S. Sumithran, M. Sono, M. Antalík, M. Fedurco, J. H. Dawson and G. Smulevich, *Arch. Biochem. Biophys.*, 2009, **489**, 68–75.
81 S. R. Yeh and D. L. Rousseau, *J. Biol. Chem.*, 1999, **274**, 17853–17859.
82 R. Pietri, A. Lewis, R. G. León, G. Casabona, L. Kiger, S.-R. Yeh, S. Fernandez-Alberti, M. C. Marden, C. L. Cadilla and J. López-Garriga, *Biochemistry*, 2009, **48**, 4881–4894.

83 J. S. Milne, L. Mayne, H. Roder, A. J. Wand and S. W. Englander, *Protein Sci.*, 1998, **7**, 739–745.
84 T. J. T. Pinheiro, G. A. Elöve, A. Watts and H. Roder, *Biochemistry*, 1997, **36**, 13122–13132.
85 T. Ying, Z. H. Wang, Y. W. Lin, J. Xie, X. Tan and Z. X. Huang, *Chem. Commun.*, 2009, 4512–4514.
86 C. M. Lett, A. M. Berghuis, H. E. Frey, J. R. Lepock and J. G. Guillemette, *J. Biol. Chem.*, 1996, **271**, 29088–29093.
87 M. Cervelli, P. Mariottini, G. Smulevich, M. Coletta and L. Fiorucci, *J. Inorg. Biochem.*, 2017, **169**, 86–96.
88 J. Gu, D. W. Shin and E. V. Pletneva, *Biochemistry*, 2017, **56**, 2950–2966.
89 C. M. Lett, M. D. Rosu-Myles, H. E. Frey and J. G. Guillemette, *Biochim. Biophys. Acta, Protein Struct. Mol. Enzymol.*, 1999, **1432**, 40–48.
90 A. M. Berghuis, J. G. Guillemette, M. Smith and G. D. Brayer, *J. Mol. Biol.*, 1994, **235**, 1326–1341.
91 S. R. Singh, S. Prakash, V. Vasu and C. Karunakaran, *J. Mol. Graphics. Modell.*, 2009, **28**, 270–277.
92 A. Schejter, T. L. Luntz, T. I. Koshy and E. Margoliash, *Biochemistry*, 1992, **31**, 8336–8343.
93 T. L. Luntz, A. Schejter, E. A. E. Garber and E. Margoliash, *Proc. Natl. Acad. Sci. U. S. A.*, 1989, **86**, 3524–3528.
94 B. A. Feinberg, L. Petro, G. Hock, W. Qin and E. Margoliash, *J. Pharm. Biomed. Anal.*, 1999, **19**, 115–125, DOI: 10.1016/S0731-7085(98)00291-X.
95 G. Battistuzzi, C. A. Bortolotti, M. Bellei, G. Di Rocco, J. Salewski, P. Hildebrandt and M. Sola, *Biochemistry*, 2012, **51**, 5967–5978.
96 L. Tognaccini, C. Ciaccio, V. D'Oria, M. Cervelli, B. D. Howes, M. Coletta, P. Mariottini, G. Smulevich and L. Fiorucci, *J. Inorg. Biochem.*, 2016, **155**, 56–66.
97 S. Casalini, G. Battistuzzi, M. Borsari, A. Ranieri and M. Sola, *J. Am. Chem. Soc.*, 2008, **130**, 15099–15104.
98 S. Casalini, G. Battistuzzi, M. Borsari, C. A. Bortolotti, A. Ranieri and M. Sola, *J. Phys. Chem. B*, 2008, **112**, 1555–1563.
99 S. Casalini, G. Battistuzzi, M. Borsari, C. A. Bortolotti, G. Di Rocco, A. Ranieri and M. Sola, *J. Phys. Chem. B*, 2010, **114**, 1698–1706.
100 C. A. Bortolotti, G. Battistuzzi, M. Borsari, P. Facci, A. Ranieri and M. Sola, *J. Am. Chem. Soc.*, 2006, **128**, 5444–5451.
101 F. Paulat and N. Lehnert, *Inorg. Chem.*, 2008, **47**, 4963–4976.
102 G. Battistuzzi, C. A. Bortolotti, M. Bellei, G. Di Rocco, J. Salewski, P. Hildebrandt and M. Sola, *Biochemistry*, 2012, **51**, 5967–5978.
103 M. Bellei, C. A. Bortolotti, G. Di Rocco, M. Borsari, L. Lancellotti, A. Ranieri, M. Sola and G. Battistuzzi, *J. Inorg. Biochem.*, 2018, **178**, 70–86.
104 G. Di Rocco, G. Battistuzzi, C. A. Bortolotti, M. Borsari, E. Ferrari, S. Monari and M. Sola, *JBIC, J. Biol. Inorg. Chem.*, 2011, **16**, 461–471.
105 K. L. Bren and H. B. Gray, *J. Am. Chem. Soc.*, 1993, **115**, 10382–10383.
106 Y. Lu, D. R. Casimiro, K. L. Bren, J. H. Richards and H. B. Gray, *Proc. Natl. Acad. Sci. U. S. A.*, 1993, **90**, 11456–11459.
107 G. Battistuzzi, M. Borsari, D. Dallari, S. Ferretti and M. Sola, *Eur. J. Biochem.*, 1995, **233**, 335–339.
108 E. L. Yee and M. J. Weaver, *Inorg. Chem.*, 1980, **19**, 1077–1079.
109 E. L. Yee, R. J. Cave, K. L. Guyer, P. D. Tyma and M. J. Weaver, *J. Am. Chem. Soc.*, 1979, **101**, 1131–1137, DOI: 10.1021/ja00499a013.
110 V. T. Taniguchi, N. Sailasuta-Scott, F. C. Anson and H. B. Gray, *Pure Appl. Chem.*, 1980, **52**, 2275–2281.
111 G. Battistuzzi, M. Borsari, M. Sola and F. Francia, *Biochemistry*, 1997, **36**, 16247–16258.
112 G. Battistuzzi, M. Borsari, L. Loschi and M. Sola, *JBIC, J. Biol. Inorg. Chem.*, 1997, **2**, 350–359.
113 G. Battistuzzi, M. Borsari, L. Loschi, F. Righi and M. Sola, *J. Am. Chem. Soc.*, 1999, **121**, 501–506.
114 L. Banci, I. Bertini, K. L. Bren, H. B. Gray and P. Turano, *Chem. Biol.*, 1995, **2**, 377–383.
115 M. R. Cheesman, C. Greenwood and A. J. Thomson, *Adv. Inorg. Chem.*, 1991, **36**, 201–255.
116 R. Schweitzer-Stenner, *J. Phys. Chem. B*, 2008, **112**, 10358–10366.
117 L. Vickery, T. Nozawa and K. Sauer, *J. Am. Chem. Soc.*, 1976, **98**, 351–357.
118 L. Vickery, K. Sauer and T. Nozawa, *J. Am. Chem. Soc.*, 1976, **98**, 343–350.
119 N. Tomášková, R. Varhač, V. Lysáková, A. Musatov and E. Sedlák, *Biochim. Biophys. Acta, Proteins Proteomics*, 2018, **1866**, 1073–1083.
120 D. W. Urry, *J. Biol. Chem.*, 1967, **242**, 4441–4448.
121 E. H. Strickland and S. Beychok, *CRC Crit. Rev. Biochem.*, 1974, **2**, 113–175.
122 A. M. Davies, J. G. Guillemette, M. Smith, C. Greenwood, A. G. P. Thurgood, A. G. Mauk and G. R. Moore, *Biochemistry*, 1993, **32**, 5431–5435.
123 H. R. Schroeder, F. A. McOdimba, J. G. Guillemette and J. A. Kornblatt, *Biochem. Cell Biol.*, 1997, **75**, 191–197.
124 N. Sanghera and T. J. T. Pinheiro, *Protein Sci.*, 2009, **9**, 1194–1202.
125 M. J. Tarlov and E. F. Bowden, *J. Am. Chem. Soc.*, 1991, **113**, 1847–1849.
126 G. Battistuzzi, M. Bellei, M. Borsari, G. Di Rocco, A. Ranieri and M. Sola, *JBIC, J. Biol. Inorg. Chem.*, 2005, **10**, 643–651.
127 M. Bellei, C. Jakopitsch, G. Battistuzzi, M. Sola and C. Obinger, *Biochemistry*, 2006, **45**, 4768–4774.
128 G. Battistuzzi, M. Bellei, M. Zederbauer, P. G. Furtmüller, M. Sola and C. Obinger, *Biochemistry*, 2006, **45**, 12750–12755.
129 G. Battistuzzi, M. Bellei, L. Casella, C. A. Bortolotti, R. Roncone, E. Monzani and M. Sola, *JBIC, J. Biol. Inorg. Chem.*, 2007, **12**, 951–958.
130 G. Battistuzzi, M. Bellei, J. Vlasits, S. Banerjee, P. G. Furtmüller, M. Sola and C. Obinger, *Arch. Biochem. Biophys.*, 2010, **494**, 72–77.
131 J. Vlasits, M. Bellei, C. Jakopitsch, F. De Rienzo, P. G. Furtmüller, M. Zamocky, M. Sola, G. Battistuzzi and C. Obinger, *J. Inorg. Biochem.*, 2010, **104**, 648–656.
132 G. Battistuzzi, J. Stampler, M. Bellei, J. Vlasits, M. Soudi, P. G. Furtmüller and C. Obinger, *Biochemistry*, 2011, **50**, 7987–7994.

133 S. Hofbauer, K. Gysel, M. Bellei, A. Hagmüller, I. Schaffner, G. Mlynek, J. Kostan, K. F. Pirker, H. Daims, P. G. Furtmüller, G. Battistuzzi, K. Djinović-Carugo and C. Obinger, *Biochemistry*, 2014, **53**, 77–89.
134 M. Paumann-Page, R.-S. S. Katz, M. Bellei, I. Schwartz, E. Edenhofer, B. Sevcnikar, M. Soudi, S. Hofbauer, G. Battistuzzi, P. G. Furtmüller and C. Obinger, *J. Biol. Chem.*, 2017, **292**, 4583–4592.
135 G. Di Rocco, A. Ranieri, C. A. Bortolotti, G. Battistuzzi, A. Bonifacio, V. Sergo, M. Borsari and M. Sola, *Phys. Chem. Chem. Phys.*, 2013, **15**, 13499.
136 X. Liu, Y. Huang, W. Zhang, G. Fan, C. Fan and G. Li, *Langmuir*, 2005, **21**, 375–378.
137 S. Monari, G. Battistuzzi, M. Borsari, G. Di Rocco, L. Martini, A. Ranieri and M. Sola, *J. Phys. Chem. B*, 2009, **113**, 13645–13653.
138 G. Battistuzzi, M. Bellei, C. A. Bortolotti and M. Sola, *Arch. Biochem. Biophys.*, 2010, **500**, 21–36.
139 S. Monari, G. Battistuzzi, M. Borsari, D. Millo, C. Gooijer, G. Van Der Zwan, A. Ranieri and M. Sola, *J. Appl. Electrochem.*, 2008, **38**, 885–891.
140 G. Battistuzzi, M. Borsari, J. A. Cowan, C. Eicken, L. Loschi and M. Sola, *Biochemistry*, 1999, **38**, 5553–5562.
141 B. Dangi, S. Sarma, C. Yan, D. L. Banville and R. D. Guiles, *Biochemistry*, 1998, **2960**, 8289–8302, DOI: 10.1021/bi9801964.
142 G. Di Rocco, F. Bernini, M. Borsari, I. Martinelli, C. A. Bortolotti, G. Battistuzzi, A. Ranieri, M. Caselli, M. Sola and G. Ponterini, *Zeitschrift fur Phys. Chemie*, 2016, **230**, 1329–1349.
143 G. Battistuzzi, M. Borsari, A. Ranieri and M. Sola, *J. Am. Chem. Soc.*, 2002, **124**, 26–27.
144 G. Battistuzzi, M. Borsari, C. A. Bortolotti, G. Di Rocco, A. Ranieri and M. Sola, *J. Phys. Chem. B*, 2007, **111**, 10281–10287.
145 S. Hofbauer, M. Bellei, A. Sündermann, K. F. Pirker, A. Hagmüller, G. Mlynek, J. Kostan, H. Daims, P. G. Furtmüller, K. Djinović-Carugo, C. Oostenbrink, G. Battistuzzi and C. Obinger, *Biochemistry*, 2012, **51**, 9501–9512.
146 V. Pfanzagl, M. Bellei, S. Hofbauer, C. V. F. P. Laurent, P. G. Furtmüller, C. Oostenbrink, G. Battistuzzi and C. Obinger, *J. Inorg. Biochem.*, 2019, **199**, 110761.
147 G. Battistuzzi, M. Borsari, J. A. Cowan, A. Ranieri and M. Sola, *J. Am. Chem. Soc.*, 2002, **124**, 5315–5324.
148 G. Battistuzzi, M. Bellei, F. De Rienzo and M. Sola, *JBIC, J. Biol. Inorg. Chem.*, 2006, **11**, 586–592.
149 G. Battistuzzi, M. Borsari, G. Di Rocco, A. Ranieri and M. Sola, *JBIC, J. Biol. Inorg. Chem.*, 2004, **9**, 23–26.
150 E. Grunwald, *J. Am. Chem. Soc.*, 1986, **108**, 5726–5731.
151 L. Liu and Q.-X. Guo, *Chem. Rev.*, 2001, **101**, 673–696.
152 L. Liu, C. Yang and Q.-X. Guo, *Biophys. Chem.*, 2000, **84**, 239–251.
153 G. Battistuzzi, M. Bellei, C. Dennison, G. Di Rocco, K. Sato, M. Sola and S. Yanagisawa, *JBIC, J. Biol. Inorg. Chem.*, 2007, **12**, 895–900.
154 E. B. Starikov, *Chem. Phys. Lett.*, 2013, **564**, 88–92.
155 E. B. Starikov and B. Norden, *J. Phys. Chem. B*, 2007, 14431–14435, DOI: 10.1021/jp075784i.
156 E. B. Starikov and B. Nordén, *Chem. Phys. Lett.*, 2012, **538**, 118–120.
157 L. Movileanu and E. A. Schiff, *Monatshefte für Chemie – Chem. Mon.*, 2013, **144**, 59–65.
158 G. Battistuzzi, M. Borsari, G. W. Canters, E. De Waal, A. Leonardi, A. Ranieri and M. Sola, *Biochemistry*, 2002, **41**, 14293–14298.
159 M. Bellei, G. Battistuzzi, S. pao Wu, S. S. Mansy, J. A. Cowan and M. Sola, *J. Inorg. Biochem.*, 2010, **104**, 691–696.
160 J. B. Soffer and R. Schweitzer-Stenner, *J. Biol. Inorg. Chem.*, 2014, **19**, 1181–1194.
161 J. M. Fox, M. Zhao, M. J. Fink, K. Kang and G. M. Whitesides, *Annu. Rev. Biophys.*, 2018, **47**, 223–250.
162 G. Battistuzzi, M. Bellei, M. Borsari, G. W. Canters, E. De Waal, L. J. C. Jeuken, A. Ranieri and M. Sola, *Biochemistry*, 2003, **42**, 9214–9220.
163 S. Monari, A. Ranieri, C. A. Bortolotti, S. Peressini, C. Tavagnacco and M. Borsari, *Electrochim. Acta*, 2011, **56**, 6925–6931.
164 E. Grunwald and C. Steel, *J. Am. Chem. Soc.*, 1995, **117**, 5687–5692.
165 D. N. LeBard and D. V. Matyushov, *J. Chem. Phys.*, 2008, **128**, 155106.
166 D. V. Matyushov, *J. Chem. Phys.*, 2013, **139**, 25102.
167 G. Battistuzzi, M. Borsari, G. Di Rocco, A. Ranieri and M. Sola, *JBIC, J. Biol. Inorg. Chem.*, 2004, **9**, 23–26.
168 D. Shortle, in *Protein Stability*, ed. C. B. Anfinsen, F. M. Richards, J. T. Edsall and D. S. B. T.-A., P. C. Eisenberg, Academic Press, 1995, vol. 46, pp. 217–247.
169 K. Dill, *Annu. Rev. Biochem.*, 1991, **60**, 795–825.
170 L. Hua, R. Zhou, D. Thirumalai and B. J. Berne, *Proc. Natl. Acad. Sci. U. S. A.*, 2008, **105**, 16928–16933.
171 P. J. Rossky, *Proc. Natl. Acad. Sci. U. S. A.*, 2008, **105**, 16825–16826.